3D Pose Estimation of Bin Picking Object using Deep Learning and 3D Matching

Junesuk Lee[1], Sangseung Kang[2] and Soon-Yong Park[1]
[1]*School of Computer Science and Engineering, Kyungpook National University, Daegu, South Korea*
[2]*Intelligent Robotics Research Division, Electronics and Telecommunications Research Institute, Daejeon, South Korea*

Keywords: Bin Picking, Pose Estimation, Object Detection, Deep Learning, 3D Matching.

Abstract: In this paper, we propose a method to estimate 3D pose information of an object in a randomly piled-up environment by using image data obtained from an RGB-D camera. The proposed method consists of two modules: object detection by deep learning, and pose estimation by Iterative Closest Point (ICP) algorithm. In the first module, we propose an image encoding method to generate three channel images by integrating depth and infrared images captured by the camera. We use these encoded images as both the input data and training data set in a deep learning-based object detection step. Also, we propose a depth-based filtering method to improve the precision of object detection and to reduce the number of false positives by pre-processing input data. ICP-based 3D pose estimation is done in the second module, where we applied a plane-fitting method to increase the accuracy of the estimated pose.

1 INTRODUCTION

With the rapid development of modern visual recognition technology, many advanced systems have been introduced to automate the works of assembly lines in large industries. Such automation is achieved by implementing high-tech robots, mainly on the seek of increasing productivity and efficiency. Consequently, the topic bin-picking has started to attract the attention of many researchers. In computer vision society, this topic is defined as "the method of estimating the pose of randomly piled-up objects, and sending pose data to robots to act accordingly."

From the past to the present, a large number of bin-picking research works have been actively conducted. Kuo et al. proposed an automatic system for object detection and pose estimation using a single depth map (Kuo et al., 2014). Object detection is based on matching key-points (using RANSAC algorithm (Schnable et al., 2007)) extracted from the depth image, where pose estimation is achieved by applying ICP algorithm (Besl and McKay, 1992). Wu et al. introduced a method to estimate object pose by using a CAD model, where they applied a voxel grid filter (Skotheim et al, 2012) to reduce the total computation time (Wu et al., 2015). Wada et al. proposed a Convolution Neural Network-based (CNN) object recognition and splitting method for objects that are stacked in narrow spaces (Wada et al., 2016). Radhakrishnamurthy et al. researched about an automated stereo bin-picking system and proposed the ATOT (Acclimatized Top Object Threshold) algorithm to identify the top-most object in a pile of occluded objects (Radhakrishnamurthy et al., 2017). Instead of using a threshold value for binarization (Otsu, 1979) through trial-and-error, they advanced their algorithm to find the correct threshold value automatically. He et al. proposed a pipeline to reduce the number of false positives in object detection (He et al, 2017). They used template matching and clustering algorithms to detect objects, and their point cloud processing algorithm to estimate the object pose.

Even though these existing methods are capable of obtaining promising results, most of them have two common drawbacks: Unstable corresponding point matchings in object detection, and insufficient 3D point data acquisition in ICP-based pose estimation. In this paper, we address these drawbacks and introduce an effective bin-picking system by utilizing computer vision, and deep-learning techniques. We divide our approach into two modules, an object detection module, and a pose estimation module. In the first module, we propose

Lee, J., Kang, S. and Park, S-Y.
3D Pose Estimation of Bin Picking Object using Deep Learning and 3D Matching.
DOI: 10.5220/0006858203180324
In *Proceedings of the 15th International Conference on Informatics in Control, Automation and Robotics (ICINCO 2018) - Volume 2*, pages 318-324
ISBN: 978-989-758-321-6

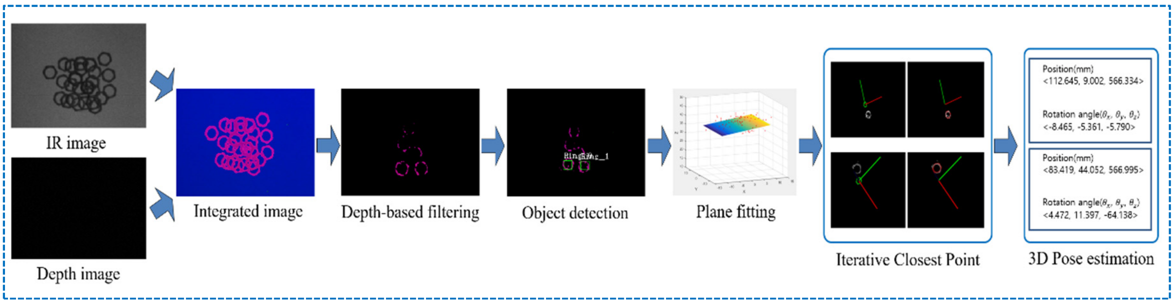

Figure 1: Proposed system flowchart.

an encoding method to integrate IR and depth images of the camera to generate a new-3-channel image and a depth-based filtering method to improve deep learning-based object detection precision. In the second module, we use the ICP algorithm to estimate the pose of the first module's detected objects. To solve insufficient 3D point data problem, we apply plane-fitting (Radu and Cousins, 2011) to move the plane equation of the surface in the direct-ion of its normal vector. This approach increased the total number of matching points of the object.

Fig. 1 shows the flow chart proposed in this paper to estimate the pose of an object. First, an infrared image and a depth image are obtained from an RGB-D camera. Then, the two images of the previous stage are integrated into one image by the proposed method. This integrated image is used as training-data to train YOLO(You only look once) v2(Redmon and Farhadi, 2017). Then, we apply the depth-based filtering proposed in this paper to this integrated image. The reason for applying this filtering is to solve the problem that it is difficult for the detector to detect an object if the objects overlap each other. Then we detect the object with a detector trained with YOLO v2. Next, the point cloud of the detected object is obtained using the perspective back-projection transformation. Then, as in section 3.1, we use PCL(Point Cloud Library)'s plane-fitting algorithm to acquire an additional point cloud of objects. Finally, we use PCL's ICP algorithm to estimate the pose of the object using the acquired point clouds and the CAD model of the object. In this paper, we study two kinds of objects. We randomly piled objects to make an experimental environment. However, we do not mix two kinds of objects in one experimental environment.

The structure of our paper is as follows. The first module: image encoding and object detection are introduced in section 2, where ICP-based pose estimation is stated in section 3. We validated the accuracy of two modules through experimental results and summarized them in section 4. Lastly, conclusions are summarized in the final section of this paper.

2 IMAGE ENCODING AND OBJECT DETECTION

2.1 Generating 3-channel Encoded Image

A time-of-flight (ToF) camera is a range imaging capable camera that resolves distance to points in 2D images. Kinect v2 is a ToF-type camera capable of producing both depth and infrared images (Butkiewicz, 2014). Even though ToF-type cameras have an illumination variant characteristic, they are less likely to be influenced by lighting conditions in indoor environments. Based on this assumption, in this paper, we created a three-channel image using depth and IR images acquired from Kinect v2 using the following method.

First, we normalize the depth value of the depth image using Eq. (1) and then assign this value to the first channel(channel$_1$).

$$\text{Channel}_1 = \frac{\text{Depth}_{\text{input}} - \text{Depth}_{\text{min}}}{\text{Depth}_{\text{max}} - \text{Depth}_{\text{min}}} \tag{1}$$

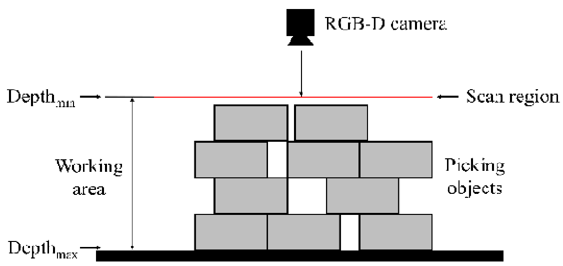

Figure 2: A graphical representation of how bins are piled-up. The RGB-D camera is mounted on top of the bin.

Fig. 2 depicts a general situation where objects are piled-up on a flat surface. Depth$_{input}$ represents the depth data obtained from the RGB-D camera, where $Depth_{min}$ and $Depth_{max}$ represent the distances to starting and end positions of the user-defined working area from the camera. The starting point is not necessarily the starting point of the first piled bin. Second, we assigned original data of the IR image to the second channel(channel$_2$). To summarize the first and second channels, the first channel is assigned a normalized depth value, and the second channel is assigned a normalized value of the pixel size of the IR image.

Finally, we used the predefined thresholds to remove the background of the IR image and assign the normalized value to the third channel(channel$_3$) using Eq. (2). This method emphasizes the shape of an object by making the difference between the object and the background large. The reason for doing this is to make the features of the object stronger when training the deep learning model. In Eq. (2), the constant value is an experimentally obtained value. Fig. 3 shows an example of the process of creating a 3-channel image using the proposed method. In Fig. 3, the right image is the IR image and the depth image, and the left image is the resulting image.

$$\text{Channel}_3 = 128 + \text{pixel\_value} \times 6 \qquad (2)$$

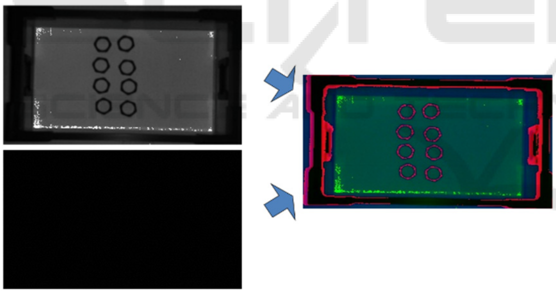

Figure 3: Creating a 3-channel image using IR image and depth image.

2.2 Depth-based Filtering

Detecting target objects when they are overlapped with each other is not an easy task. Overlapping results in changing the characteristics of individual objects. This is a very common issue in objects with holes in their center. For example, as in the case of Fig. 4, the object detector falsely recognizes two or more overlapping objects as a single object.

We propose a recursive depth-based filtering method to solve this problem. This is a method of acquiring data between distance threshold from the camera position in the work area. This method applies to the only channel$_3$ in the encoded image.

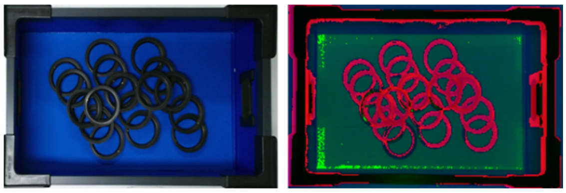

(a) (b)

Figure 4: Examples of target objects piled up in a rectangle box (a) color image (b) proposed encoding image.

Taking Fig. 2 as an example, our proposed filtering method is to remove data located farther away than the red line based on the camera position. This red line indicates the vertical search area from the camera position to the distance threshold. The data removal method is to set the pixel having a value greater than the distance threshold to zero. In the next step, this filtered image is used to detect the object using the object detector. When this task is completed, the distance threshold is incremented by 1 mm to repeat the task. We set the initial distance threshold to $Depth_{min}$ and the maximum value to $Depth_{max}$.

This process is performed recursively until all the objects are detected. Fig. 5 (a) shows the image before depth-based filtering is applied. Fig. 5(b) shows an example that depth-based filtering is applied to the image that captures the situation where objects overlap each other. The red circle in Fig. 5(b) represents the target object detected in the search region. Pixels which depth is larger than the threshold value are regarded as background and represented with blue. This representation allows to easily identify objects even they overlap with each other.

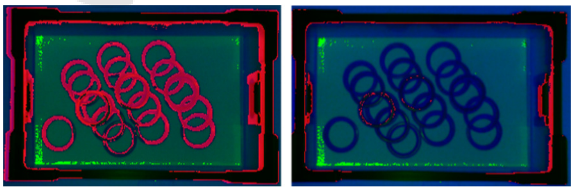

(a) (b)

Figure 5: Depth filtering (a) before depth-based filtering (b) after depth-based filtering.

2.3 Target Object Detection using Deep Neural Network

In this paper, we trained the object detector using the YOLO v2 (Redmon and Farhadi, 2017) library. The YOLO v2 library uses the Dartnet-19 model. This model has 19 convolutional layers and 5 maxpooling layers. We have collected training data as shown in Fig. 6(a) to train this deep learning model. Fig. 6(b) shows the labeling information of the training data (Fig. 6(a)). In this paper, the input image of the object detector is the depth-based filtered image and the output is the area of the detected object. Fig. 7 shows an example of the results of detecting objects using an object detector.

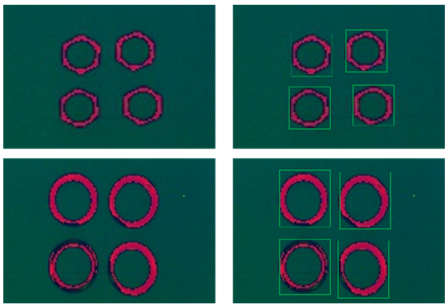

(a) (b)

Figure 6: Example of training data, (a) Training data (b) Labelling image of training data.

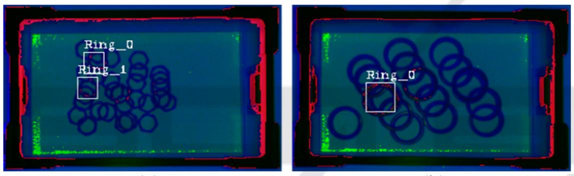

(a) (b)

Figure 7: Object detection examples using YOLO v2, (a) detected object regions of hexagonal rings (b) detected object regions of circular rings.

Occasionally, objects are tilted in the working environment. If depth-based filtering is applied in this case, the result as shown in Fig. 8(a) is output. However, the object detector we trained do not detect the object. Because we did not train an object like Fig. 8(a). If an object is not detected, depth-based filtering increases the depth threshold. When it looks like Fig. 8(b), the detector detects the tilted object.

(a) (b)

Figure 8: A case with an inclined object, (a) Object detector does not detect the object (b) After increasing the depth threshold, the object detector detects the object.

3 3D POSE ESTIMATION OF TARGET OBJECTS

3.1 Plane Fitting of the Object Top

Once the object regions are detected, we use the ICP algorithm in each object region to estimate the pose of the objects. We acquire a 3D point cloud using the perspective back-projection transformation formula for the region detected in the previous step. This point cloud is matched with the 3D CAD model of the object to find the 3D rotation and translation. The model of the object is also represented by 3D points. In general, ICP algorithm works better if the number of 3D points of the object is large. There arises a problem of insufficiently acquiring the perspective back-projection-converted 3D points because the pixels exist only in the upper part of the object in the 2D image. Therefore, in this paper, we employ a plane fitting method to acquire more 3D points for the target object.

Suppose we obtain the 3D point clouds for a detected target object which is reconstructed from the object region in the depth image. An example is shown in Fig. 9(a). This point cloud is represented as P=$\{(x_1, y_1, z_1), \dots, (x_K, y_K, z_K)\}$. The plane equation (Eq. (3)) is fitted to this point cloud as shown in Fig. 9(b). The direction of the normal vector $\vec{n}$ as in Eq. (4) is always opposite to the coordinate origin because c and z values are positive in this equation. To obtain enough 3D points from the depth, the fitted plane is shifted along the normal direction by a short length (δ) as shown in Fig. 9(c). Then, more points which satisfy Eq. (5) are added to the point clouds $\mathcal{P}$. In Eq. (5), $\mathcal{U}$ is uniform distribution.

$$ax + by + cz + d = 0 \ (c \geq 0, z \geq 0) \tag{3}$$

$$\vec{n} = (a, b, c) \tag{4}$$

$$ax_k + by_k + cz_k + (d + \delta) \leq 0 \text{ with } k \sim \mathcal{U}\{1, K\} \tag{5}$$

In summary, once, the plane equation as shown in Fig. 9(b) is obtained through the plane fitting for the point cloud of the object as shown in Fig. 9(a). Then, the plane equation as shown in Fig. 9(b) is moved in parallel to the normal vector direction by a certain size(δ). We acquire closer points from the plane relative to the origin and use it as a data set for ICP algorithm. The origin indicates the position of the camera. By applying this method, we can acquire more 3D points for the object than before.

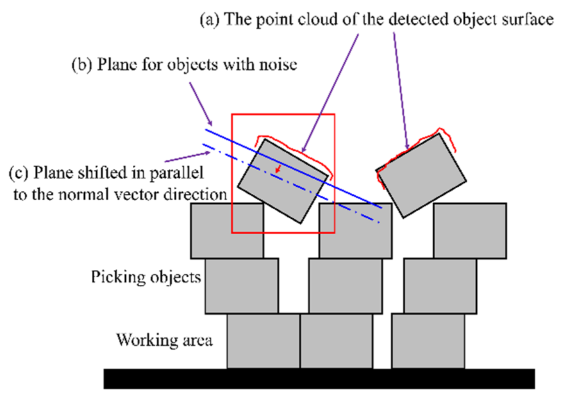

Figure 9: Plane fitting and Shifting along the plane normal direction.

3.2 3D Pose of Target Object

The pose of a target object means the 3D transformation of the object from the origin of the depth sensor. The 3D pose of target object must be known to perform the picking task of a robot system. The 3D pose of a target object is estimated by the following method.

First, we create 3D models of the two target objects. The 3D target models are also point clouds data which has the same scale with the target objects. In Fig. 10(a), one of the target models is placed at the coordinate origin in green color. The coordinate origin is defined as the coordinate of the RGB-D camera used in experiments.

Next, the point cloud of the object obtained through the plane shift method is matched with the point cloud of the target model using the ICP algorithm. The pose of the object is estimated through the translation and rotation matrices of the 3D transformation derived by the ICP algorithm.

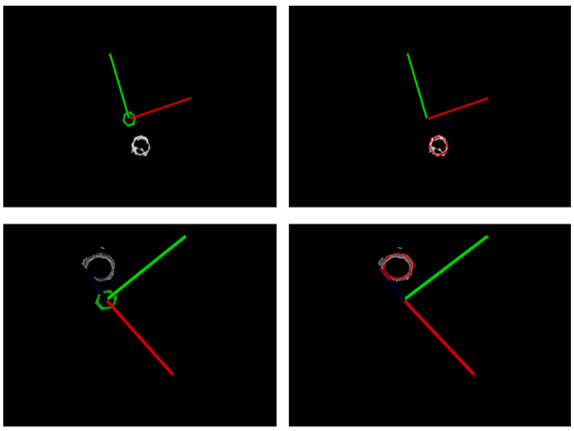

(a) (b)

Figure 10: Two examples of ICP matching (a) Before 3D matching (b) After 3D matching.

In Fig. 10(b), the target model, red-colored points, is matched with the target object, white-colored points, after applying the ICP algorithm.

4 EXPERIMENT RESULTS

4.1 Experiment Environment

To verify the performance of the proposed system, an experimental set is constructed as shown in Fig. 11(a). As target object two types of ring are used, hexagonal ring(Fig. 11(b)) and circular ring(Fig. 11(c)). The hexagonal ring has 5mm height and 45mm diameter, and there is a circular hole of diameter 30mm. The circular ring has 10mm height and 70mm diameter, and there is a circular hole of diameter 55mm.

The number of training data is shown in Table 1 and it is trained by YOLO v2 library. The experimental method is as follows. First, we detect the target objects in depth images by the trained detector. Then, a target object is randomly selected from among the detected objects. After obtaining the 3D pose information of the object, it is manually removed to simulate robotic bin picking. The simulated picking task is repeated until all target objects are removed and no object is detected. In this experiment, we excluded the case where the object was largely inclined.

(a) (b) (c)

Figure 11: (a) Experimental setup (b) Hexagonal ring (c) Circular ring.

Table 1: Number of Training Data.

	Training image	Test image
Hexagonal ring	454	323
Circular ring	283	207

4.2 Experiment Results

Table 2 and Table 3 show the results of pose estimation of two types of target objects. The target objects are randomly placed in a rectangle box. The number of object in a pile is 30 for the hexagonal object, 20 for the circular object. In each object type, experimental tests are done in five times. The single test consists of picking all detected objects out of the box.

TP(True Positive) in Tables 2 and Table 3 are cases that the following two conditions are satisfied. The first condition is that when the target model, transformed to the target object by ICP algorithm, is projected onto the image of the target. In case of correct estimation, the projected image is exactly matched with the image of the target object. The second condition is when a target object is detected in the object piled, it must be one of the topmost objects.

FP(False Positive) means the following two cases. The first case refers to a situation in which an object other than the topmost object is detected in the object piled. The second case refers to a case that a detected object region overlaps two objects.

Fig. 12 shows some of the experiment results. Fig. 12(a) shows object regions decided by the deep neural network. Fig. 12(b) shows the pose between the target model and target object before and after ICP algorithm. The rotation and translation of the object pose are shown in Fig. 12(c).

Table 2: Experimential results on hexagon al rings.

	TOTAL	TP	FP	Precision(%)
TEST 1	30	25	5	83.3
TEST 2	30	26	4	86.6
TEST 3	30	26	4	86.6
TEST 4	30	26	4	86.6
TEST 5	30	25	5	83.3
	150	128	22	85.3

Table 3: Experimental results on circular rings.

	TOTAL	TP	FP	Precision(%)
TEST 1	20	17	3	85.0
TEST 2	20	18	2	90.0
TEST 3	20	17	3	85.0
TEST 4	20	17	3	85.0
TEST 5	20	17	3	85.0
	100	86	14	86.0

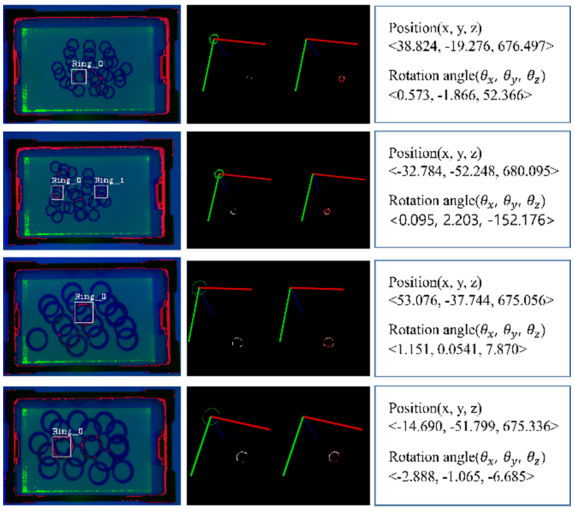

(a) (b) (c)

Figure 12: (a) Object detection (b) 3D matching (c) Pose estimation.

5 CONCLUSION

In this paper, we propose a method for estimating the 3D pose of target objects in an environment where objects are randomly piled up. We proposed an image encoding method of integrating a depth image and an infrared image which are robust to illumination changes. We trained and detected encoded images by YOLO v2. However, if objects with holes in the center are randomly piled up, there is a problem that it is difficult to detect because objects appear to cover each other and the middle part is filled with something else. We have solved this problem with the proposed depth-based filtering method. Furthermore, we proposed a method of acquiring more 3D points by both plane fitting algorithm and plane shift to obtain better results of ICP algorithm. Finally, we estimated the pose of the objects by ICP algorithm.

ACKNOWLEDGEMENTS

This research was supported by MoTIE and Industrial Core Technology Development Program of Korea Evaluation Institute of Industrial Technology (KEIT) (10063413)

REFERENCES

Kuo, H. Y., Su, H. R., Lai, S. H., 2014. 3D Object Detection and Pose Estimation from Depth Image for Robotic Bin Picking, *IEEE International Conference on Automation Science and Engineering (CASE),* pp. 1264-1269.

Schnable, R., Wahl, R. and Klein, R., 2007. Efficient RANSAC for point-cloud shape detection, *Computer Graphics Forum (CGF),* Vol. 26, no. 2, pp. 214-226.

Besl, P. J., and McKay, N. D., 1992. Method for registration of 3-D shapes, *Sensor Fusion □: Control Paradigms and Data Structures*, vol. 1611, pp. 586-607.

Wu, C. H., Jiang, S. Y., and Song, K. T., 2015. CAD-Based Pose Estimation for Random Bin-Picking of Multiple Objects Using a RGB-D Camera, *IEEE 15th International Confrence on Control, Automation and Systems (ICCAS),* pp. 1645-1649.

Skotheim, Ø, Lind, M., Ystaard, P., and Fjerdingen, S. A., 2012. A Flexible 3D object localization system for industrial part handling, *IEEE/RSJ International Conference on Intelligent Robots and Systems (IROS),* pp. 3326-3333.

Wada, K., Murooka, M., Okada, K., and Inaba, M., 2016. 3D Object Segmentation for Shelf Bin Picking by Humanoid with Deep Learning and Occupancy Voxel Grid Map, *IEEE-RAS 16th International Conference on Humanoid Robots (Humanoids),* pp. 1149-1154.

Radhakrishnamurthy, H. C., Murugesapandian, P., Ramachandran, N., and Yaacob, S., 2017. Stereo Vision System for A Bin Picking Adept Robot, *Malaysian Journal of Computer Science*, vol. 20, no. 1, pp.91-98.

Otsu, N., 1979. A threshold selection method from gray level histograms, *IEEE transactions on systems, man, and cybernetics* 9.1, pp. 62-66.

He, R., Rojas, J., and Guan, Y., 2017. A 3D Object Detection and Pose Estimation Pipeline Using RGB-D images, *arXiv preprint arXiv::1703.03940*.

Radu, R. B., and Cousins, S., 2011. 3D is here: Point Cloud library (PCL), *IEEE International Conference on Robotics and automation (ICRA),* pp. 1-4.

Butkiewicz, T., 2014. Low-cost coastal mapping using Kinect v2 time-of-flight cameras, *IEEE Oceans-ST*, pp. 1-9.

Redmon, J., and Farhadi, A., 2017. YOLO9000:Better, Faster, Stronger, *arXiv preprint*.